Electronic Supplementary Information:

Solvothermal Synthesis of Sn_3N_4 as a High Capacity Sodium-Ion Anode: Theoretical and Experimental Study of its Storage Mechanism

Samuel D. S. Fitch,[a] Giannantonio Cibin,[b] Steven P. Hepplestone,[c] Nuria Garcia-Araez[a] and Andrew L. Hector[a]

[a] School of Chemistry, University of Southampton, Southampton SO17 1BJ, UK
[b] Diamond Light Source Ltd, Diamond House, Harwell Science and Innovation Campus, Didcot, Oxfordshire OX11 0DE, UK
[c] School of Physics and Astronomy, University of Exeter, Stocker Road, Exeter, EX4 4QL UK

Contents

Fig. S7 Comparison of the XRD of the microcrystalline Sn_3N_4 electrode as a function of cell potential and the ICSD database pattern of Sn_3N_4, Sn and SnO_2.

Fig. S8 Fourier transforms of K^3-weighted Sn K-edge EXAFS during initial and final states of the first reduction of microcrystalline Sn_3N_4. The data of $Na_{15}Sn_4$ and Na_4Sn from the ICSD database is also included for comparison. Grey vertical lines indicate the radial distance of Sn-N bonds with Sn in tetrahedral or octahedral sites, and the pink vertical line indicate Na-Sn bond distance.

Fig. S9 Ex-situ Raman spectrum of a microcrystalline Sn_3N_4 electrode cycled to 10 mV in a Na half-cell. The spectrum does not show any characteristic bands that could be ascribed to NaN_3 or Na_2N_2 formation.

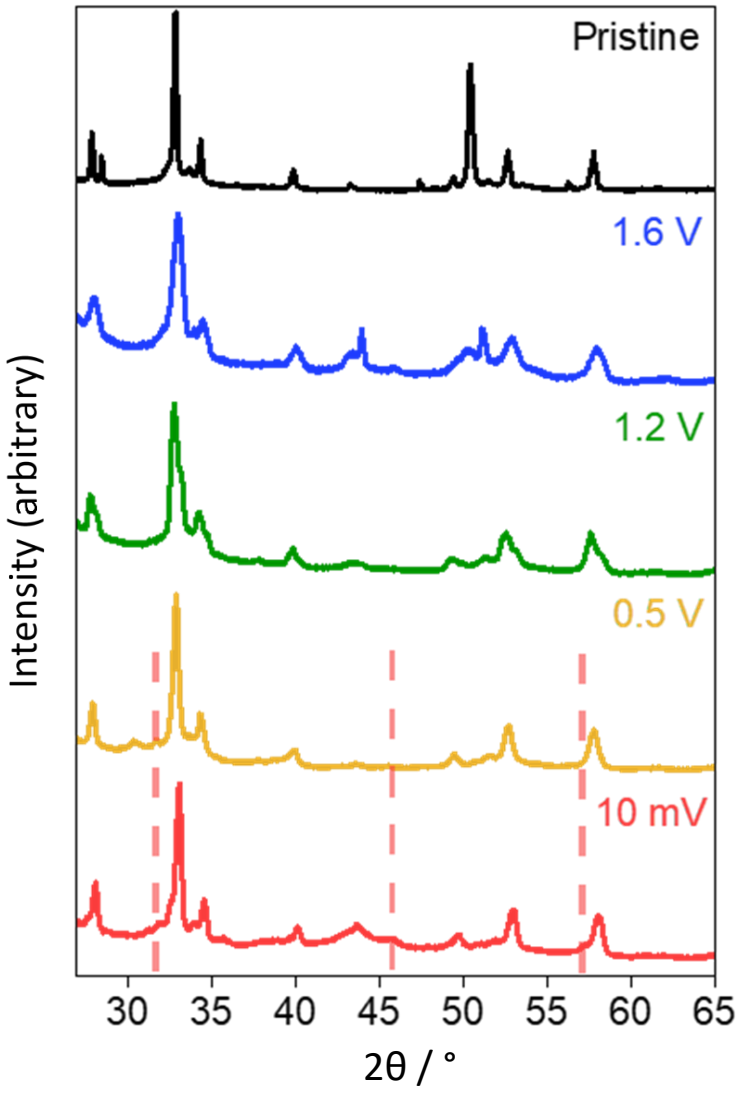

Fig. S1 *Ex situ* diffraction patterns of microcrystalline Sn_3N_4 electrodes during the initial sodiation reaction in Na half-cells. The electrodes have been prepared without homogenising the ink. Dashed red lines indicate Sn reflections observed at lower potentials during the initial reduction.

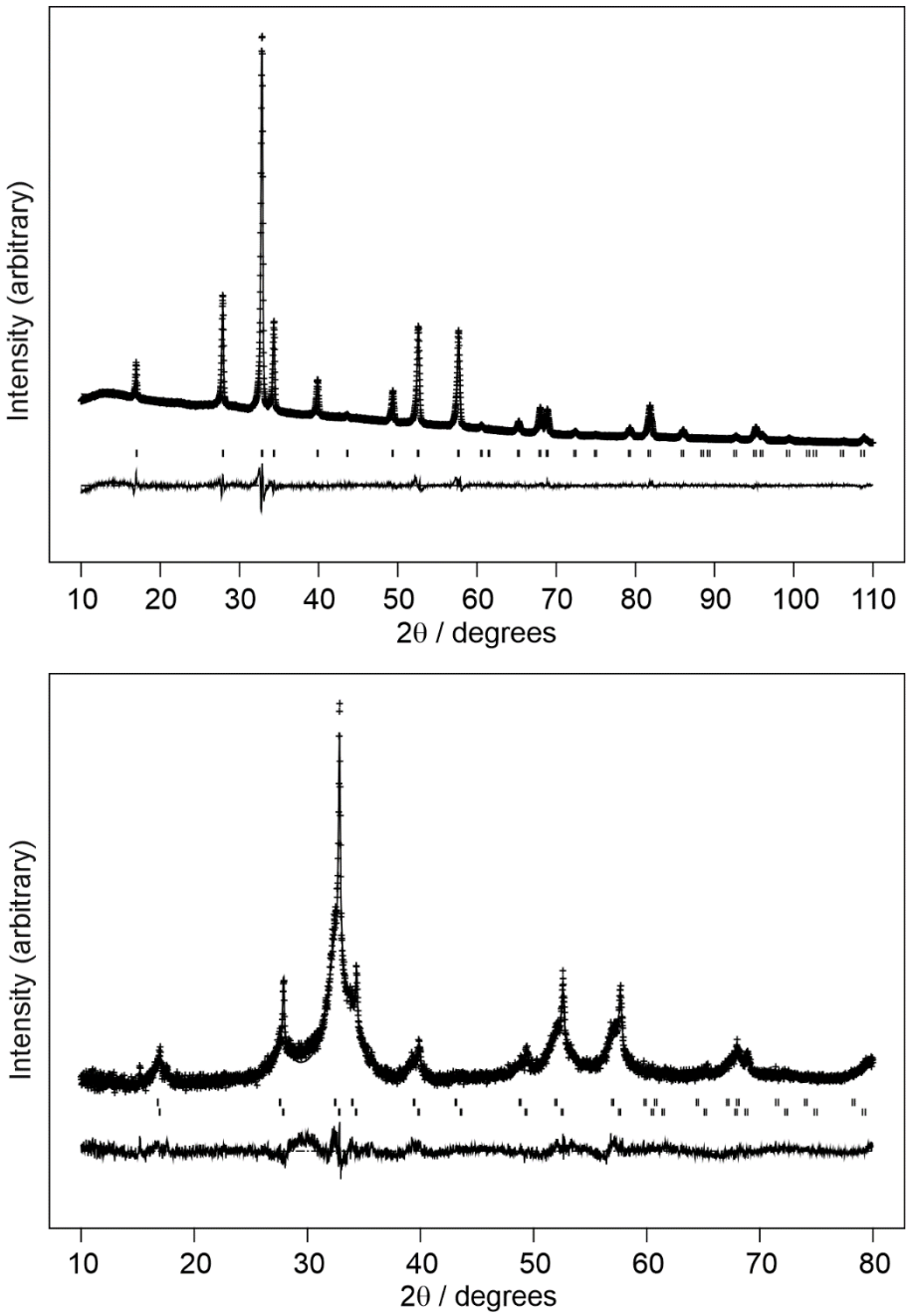

Fig. S2 Rietveld fits for microcrystalline Sn_3N_4 (**top**, one phase) and nanocrystalline Sn_3N_4 (**bottom**, two phases). (+) Indicate collected data points. Upper continuous line is the calculated profile and lower continuous line is the difference. Tick marks show allowed reflection positions for Sn_3N_4.

Table S1 Fitted parameters from the Rietveld fit to the XRD patterns for nanocrystalline and microcrystalline Sn_3N_4.

Material / Parameter	"Microcrystalline" Sn_3N_4	"Nanocrystalline" Sn_3N_4	
		Minor component	Major Component
R_{wp} / %	5.0	9.4	
R_p / %	3.4	7.4	
Wt %	100	13.2(4)	86.8(2)
a / Å	9.0549(2)	9.0514(4)	9.139(2)
Crystallite size / nm	310(40)	137(13)	5.950(9)
Sn1 ($^1/_8$,$^1/_8$,$^1/_8$) U_{iso} / Å^2	0.0231(6)	0.0102(10)	0.0102(10)
Sn2 (½,½,½) U_{iso} / Å^2	0.0234(5)	0.0102(10)	0.0102(10)
N (x,x,x) x-value	0.2600(6)	0.263(3)	0.261(2)
N (x,x,x) U_{iso} / Å^2	0.008(2)	0.02	0.02

Table S2 Results of the EXAFS fit for nanocrystalline Sn_3N_4 and microcrystalline Sn_3N_4 .

Coordination	**Microcrystalline EXAFS data analysis**		**Nanocrystalline EXAFS data analysis**		**Model crystallographic data**
Sn(1)-N (tetrahedral)	R_r / Å	2.028 ± 0.019	R_r / Å	2.077 ± 0.039	2.105
	σ_Γ^2 / Å	0.0030 ± 0.0021	σ_Γ^2 / Å	0.0043 ± 0.0029	-
Sn(2)-N (octahedral)	R_r / Å	2.137 ± 0.015	R_r / Å	2.182 ± 0.0234	2.177
	σ_Γ^2 / Å	0.0070 ± 0.0029	σ_Γ^2 / Å	0.0070 ± 0.0055	-

Table S3 The formation energy, E_f, of various reactions of Na insertion and substitution in bulk Sn_3N_4 using PBE functional. The values of formation energies are given per Na atom.

Atom/Defect type	Site label	Coordinates	E_f in eV PBE (HSE06)	Description
Sn_{tet}	8a	⅛,⅛,⅛	-	Tetrahedral Sn sites
Sn_{oct}	16d	½,½,½	-	Octahedral Sn sites
N	32e	¼, ¼, ¼	-	N sites
Interstitial	48f	0.35, ⅛,⅛	3.76 (3.37)	Tetrahedral Na interstitial edge linking to one SnN_6 octahedron and one SnN_4 tetrahedron.
Interstitial	16c	½,0,½	1.68	Octahedral Na interstitial face linking to one SnN_4 tetrahedron and edge linking to two SnN_6 octahedra.
Interstitial	32e	0.4,0.1,0.6	3.76	Tetrahedral Na interstitial face linking to two SnN_6 octahedra and edge linking to one SnN_4 tetrahedron.
Interstitial	48f	⅛,⅛,⅜	3.78	Tetrahedral Na interstitial face linking to two SnN_6 octahedra and edge linking to one SnN_4 tetrahedron.
Interstitial	16c	¼, 0, ¼	2.36	Octahedral Na interstitial face linking to one SnN_4 tetrahedron and edge linking to two SnN_6 octahedra. Initial structure resulted in distortion of Sn_3N_4 lattice.
Interstitial	16c	½, ¼ ,¾	-0.53	Octahedral Na interstitial face linking to two SnN_4 tetrahedra edge linking to four SnN_6 octahedra. Unit cell doubled along a so the ¼,¼,¾ interstitial site becomes ½,¼,¾ based on the standard unit cell
Substitution	16d	0,0,0	4.47	Substitution of Na into one octahedral Sn site.
Substitution	8a	⅛, ⅛, ⅛	4.33	Substitution of Na into one tetrahedral Sn site.
Substitution	32e	¼, ¼, ¼	8.68	Substitution of Na into one N site.
Double interstitial	32e & 16c	0.4,0.1,0.6 & ½ , 0, ½	1.89	Octahedral Na interstitial face linking to one SnN_4 tetrahedron and edge linking to two SnN_6 octahedra. & Octahedral Na interstitial face linking to one SnN_4 tetrahedron and edge linking to two SnN_6 octahedra.
Double interstitial	16c & 16c	½,0,½ & ¼, 0 ¼	1.28	Octahedral Na interstitial face linking to one SnN_4 tetrahedron and edge linking to two SnN_6 octahedra & Octahedral Na interstitial face linking to one SnN_4 tetrahedron and edge linking to two SnN_6 octahedra. Initial structure.

Table S4 The formation energy, E_f, of various reactions of Na insertion and substitution on the surface of Sn_3N_4 using PBE functional. The slab modelled was 14 Å in thickness and consisted of a 1x1 surface reconstruction. The values of formation energies are given per Na atom.

Atom/Defect type	E_f PBE (eV)	Description
Na adsorbent	-3.58	Na atom adsorbed to surface of Sn_3N_4 slab (above tetrahedral site)
Interstitial	-3.36	Na interstitial X ~2Å below the surface
Interstitial	-1.74	Na interstitial X ~7Å below the surface
Na substitution for Sn	-1.90	Na substituted for surface tetrahedral Sn
Na substitution for Sn	-0.59	Na substituted for subsurface tetrahedral Sn (below surface monolayer)

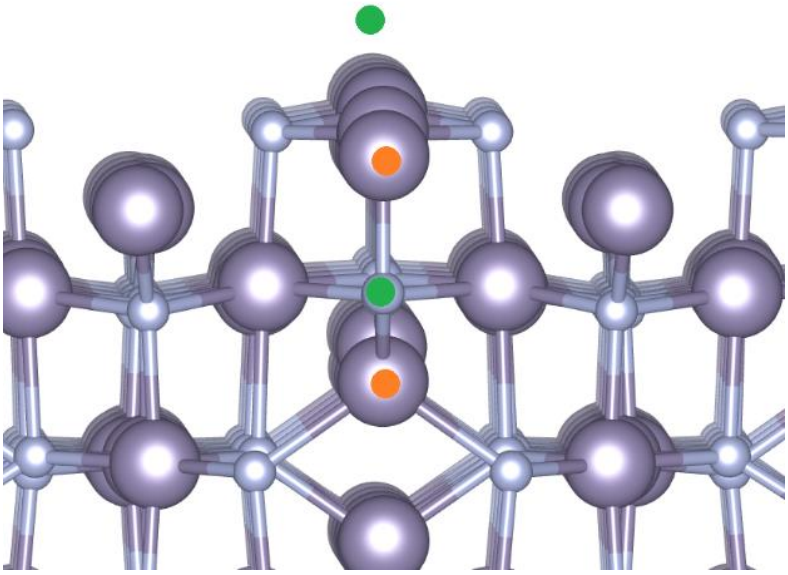

Fig. S3. A ball and stick representation of the Sn_3N_4 surface structure. The large purple spheres are Sn; the smaller purple spheres are nitrogen. The Na interstitials are shown with green dots. The two substitutional sites for the substitution of Sn by Na are highlighted with orange dots.

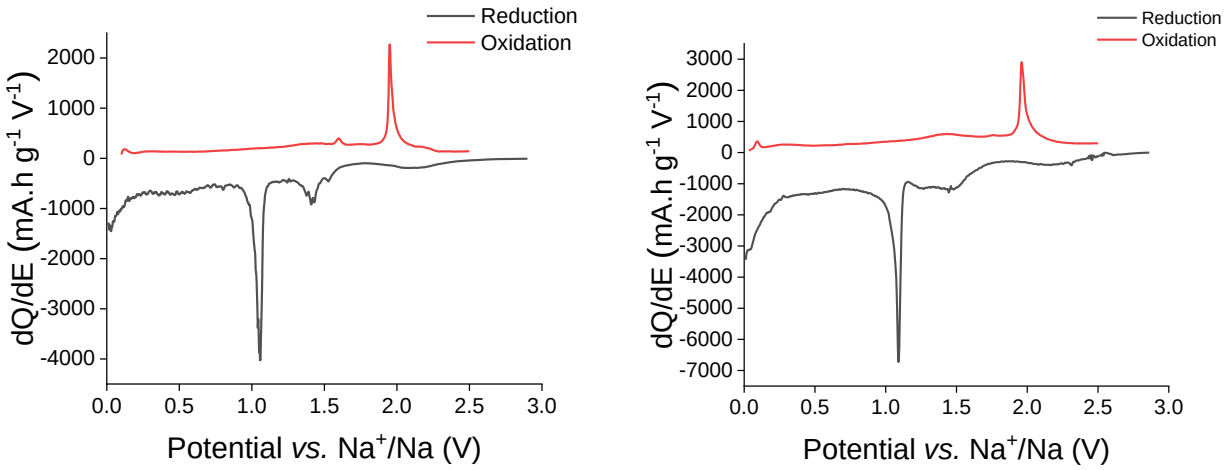

Fig. S4 Derivative capacity plot computed from the initial galvanostatic cycle of microcrystalline (**Left**) and nanocrystalline (**Right**) Sn_3N_4 at a specific current of 50 mA g^{-1}.

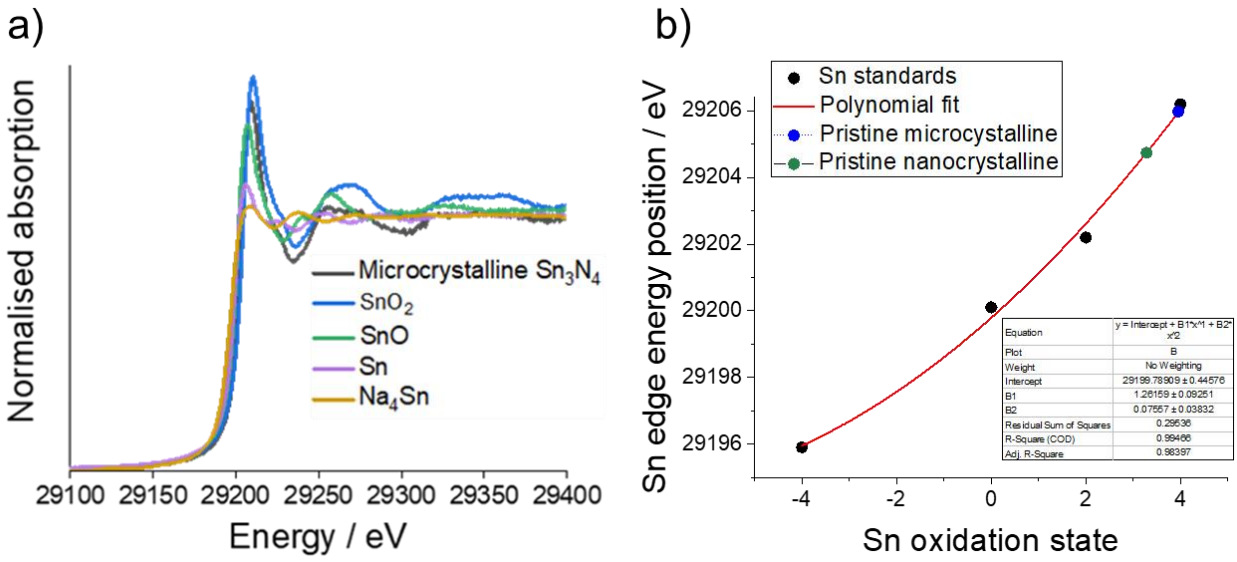

Fig. S5 (a) Sn-K edge XANES of known Sn standards and pristine microcrystalline Sn_3N_4 electrode. **(b)** Calibration of Sn-K edge energies *vs.* oxidation state.

Table S5 Average oxidation state, as evaluated from the Sn K-edge energies, of microcrystalline Sn_3N_4 electrodes as a function of cell potential during reduction and oxidation.

Sample *vs.* (Na^+/Na)		Oxidation state (Sn)	Sn K-edge energy
Pristine		3.7	29205.5
reduction	1.6 V	3.1	29204.4
	1.2 V	2.9	29203.8
	1.0 V	2.5	29203.4
	0.5 V	1.3	29201.2
	10 mV	-0.1	29199.6
oxidation	0.1 V	0.9	29200.7
	0.75 V	1.5	29301.3
	1.5 V	2.8	29203.9
	2.5 V	3.5	29205.2

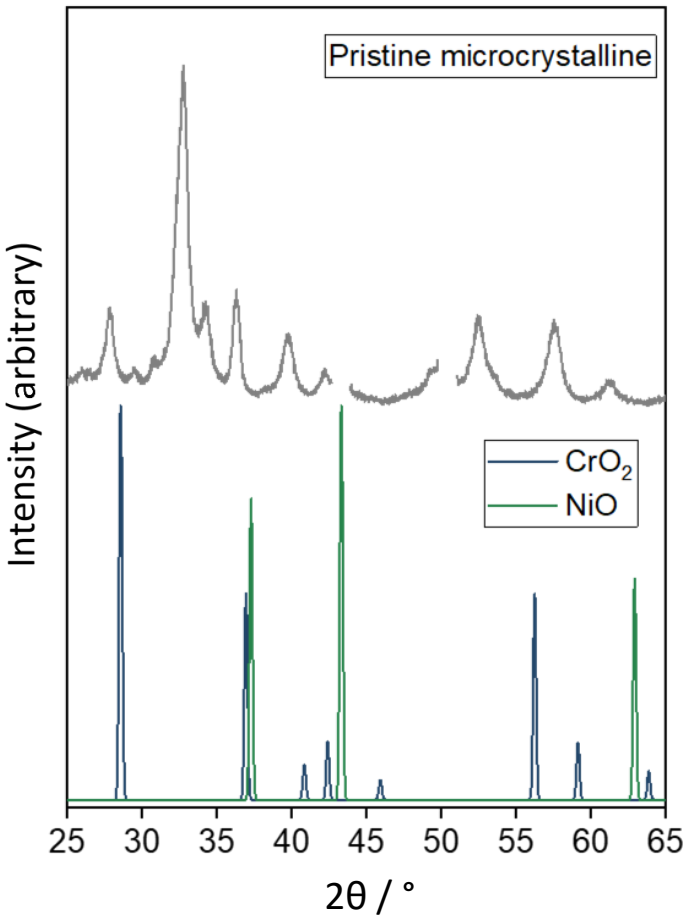

Fig. S6 Comparison of the XRD of the pristine microcrystalline Sn_3N_4 electrode and the ICSD database pattern of CrO_2 and NiO.

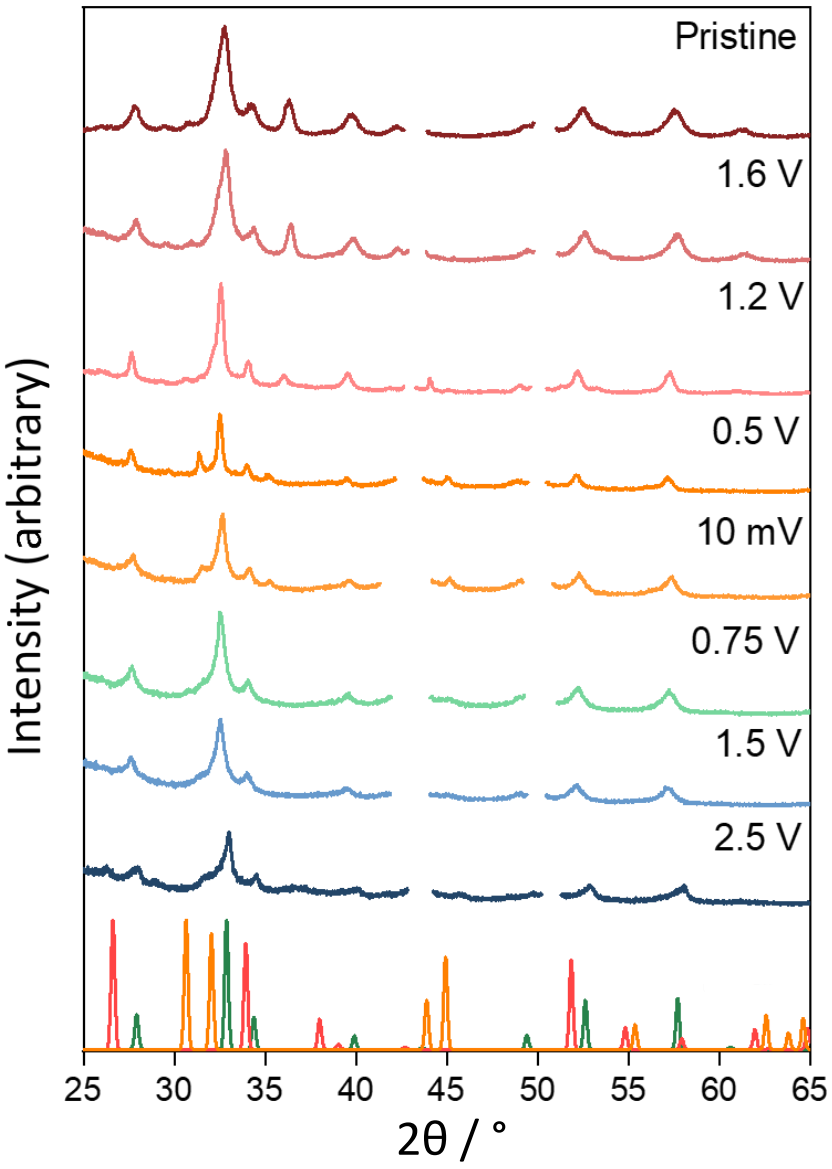

Fig. S7 Comparison of the XRD of the microcrystalline Sn_3N_4 electrode as a function of cell potential and the ICSD database pattern of Sn_3N_4 (green) Sn (orange) and SnO_2 (red).

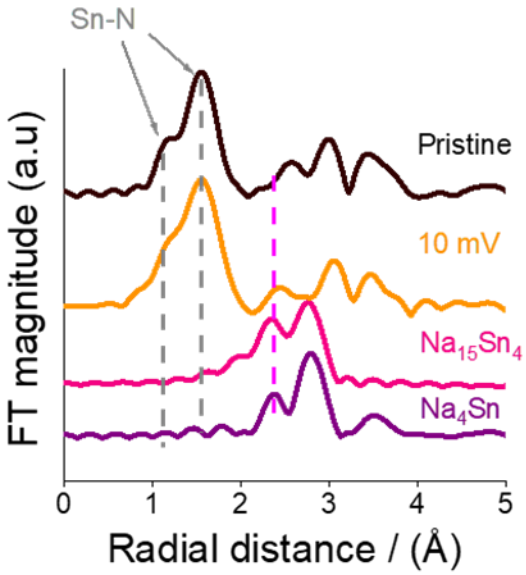

Fig. S8 Fourier transforms of K^3-weighted Sn K-edge EXAFS during initial and final states of the first reduction of microcrystalline Sn_3N_4. The data of $Na_{15}Sn_4$ and Na_4Sn from the ICSD database is also included for comparison. Grey vertical lines indicate the radial distance of Sn-N bonds with Sn in tetrahedral or octahedral sites, and the pink vertical line indicate Na-Sn bond distance.

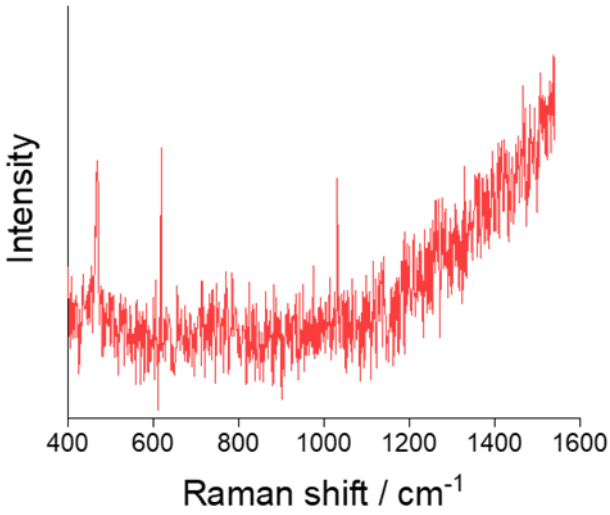

Fig. S9 Ex-situ Raman spectrum of a microcrystalline Sn_3N_4 electrode cycled to 10 mV in a Na half-cell. The spectrum does not show any characteristic bands that could be ascribed to NaN_3 or Na_2N_2 formation.